Exploring the Promotion of Synthons of Choice: Halogen Bonding in Molecular Lanthanide Complexes Characterized via X-ray Diffraction, Luminescence Spectroscopy, and Magnetic Measurements

Korey P. Carter,[a] Simon J. A. Pope,[b] Mark Kalaj,[a] Rebecca J. Holmberg,[c] Muralee Murugesu,[c] and Christopher L. Cahill*[a]

Dedicated to Professor Thomas Schleid on the Occasion of his 60th Birthday

Abstract. Promotion of a synthon of choice for the non-covalent assembly of lanthanide tectons represents both a noteworthy challenge and opportunity within Ln^{III} hybrid materials. We have developed a system, wherein some control can be exercised over supramolecular assembly and, as part of continued efforts to improve this process we have generated a family of ten new lanthanide (Ln = Sm^{3+} – Lu^{3+}) 2,4,6-trichlorobenzoic acid-1,10-phenanthroline molecular complexes. Delineation of criteria for promoting assembly via halogen based interactions was introduced previously and is refined herein based on the characterization of complexes **1**–**10** via single-crystal X-ray diffraction. Direct comparison of means of supramolecular assembly for **1**–**10** with isostructural *Ln*-*p*-chlorobenzoic acid-1,10-phenanthroline analogues verifies that increasing the number of halogen atoms at the periphery of a tecton is one route that increases the frequency of halogen bonding interactions. Additionally, solid-state visible and near-IR photoluminescence and luminescent lifetime data were collected for complexes **1** (Sm^{3+}), **2** (Eu^{3+}), **4** (Tb^{3+}), **5** (Dy^{3+}), **6** (Ho^{3+}), **7** (Er^{3+}), and **9** (Yb^{3+}) and characteristic emission was observed for all complexes except **6**. Further, direct current magnetic susceptibility measurements were carried out for complexes **5** (Dy^{3+}) and **7** (Er^{3+}), and two slow magnetic relaxation processes were characterized using alternating current magnetic susceptibility measurements for **5**.

Introduction

Supramolecular chemistry within lanthanide hybrid materials has been explored rather extensively,[1] yet remains a topic of continued interest as it presents an alternative route to accessing many of the diverse properties of lanthanide containing materials including luminescent bioprobes,[2] non-linear optics,[3] and Single-Molecule Magnets (SMMs).[4] These applications manifest as a result of the characteristic luminescent and magnetic behavior of the rare-earth elements, and efficient sensitization via luminescent antenna and precise orientation of the anisotropic axes of both the ligands and the Ln^{3+} cations were two criteria that we took into consideration when selecting ligands for this study. Harnessing the capabilities of lanthanide metal cations, such that one may selectively tune resulting properties, involves exercising some level of control over the first coordination sphere of the Ln^{3+} ions, which is a topic our group has recently probed.[1f,1g,5] One route that has proven successful is a dual-ligand strategy wherein a chelating N-donor "caps" the central Ln^{3+} metal atoms and halogen functionalized benzoic acid ligands then complete the Ln^{3+} first coordination environment, subsequently "linking" Ln^{3+} ions into discrete mono- or polynuclear units.[1d,5a] This approach is based on the formation of a *molecular* Ln^{3+} complex (or "tecton"), which will then be assembled through chemically robust, attractive motifs ("synthons") made possible by halogen atoms at the complex's periphery.

In a recent study, we focused on halogen bonding as a supramolecular synthon in a family of rare-earth molecular complexes and found that one way to promote halogen bonding as a means of assembly was simply to increase the number of halogen atoms at the periphery of the molecule.[5d] Herein we aimed to verify this premise via the synthesis and characterization of lanthanide complexes analogous to those prepared previously,[5b] with only the number of halogen atoms at the periphery of the tecton changing. This aim was successful and as a consequence we describe the synthesis, crystal structures, visible and near-IR luminescent properties, and magnetic behavior (for the Dy^{3+} and Er^{3+} species) for a family of ten molecular lanthanide materials featuring both 2,4,6-trichlorobenzoic acid (246triClBA) and 1,10-phenanthroline (phen). The dimeric tectons of complexes **1**–**10** are iso-

* Dr. C. L. Cahill E-Mail: cahill@gwu.edu
[a] Department of Chemistry
The George Washington University
800 22nd Street
NW, Washington, D.C. 20052, USA
[b] School of Chemistry, Main Building
Cardiff University
Cymru Wales, CF10 3AT, U.K
[c] Department of Chemistry and Biomolecular Sciences
University of Ottawa
10 Marie Curie
Ottawa, ON, Canada K1N 6N5

structural with structure type III complexes from a previous study,[5b] and each feature a fixed local geometry, wherein supramolecular synthons (halogen–halogen or halogen–π) link the molecular tectons into extended two-dimensional topologies.

Results and Discussion

Description of Structures

Single crystal X-ray crystallography analyses revealed one unique structure type in this series of molecular complexes. The structure type can be described as a binuclear species, and a representative example (complex **4**) is presented in detail.

[Ln(C12H8N2)(C7H2Cl3O2)3]2 (Ln = Sm3+ – Lu3+) (1–10) Structure Type I

Complexes **1**–**10**, $[Ln(C_{12}H_8N_2)(C_7H_2Cl_3O_2)_3]_2$, are isomorphous and crystallize in the space group *P*1. As **1**–**10** are also isostructural with *Ln*-*p*-chlorobenzoic acid (*p*ClBA)-phen complexes we have described previously,[5b] local structures are not described, yet as significant differences in modes of supramolecular assembly *are* observed, such are described in detail for complex **4**.

The global structure of **4** (Figure 1), features chains of terbium dimers (propagating along approximately the [001] direction) formed via bifurcated halogen–halogen interactions between chlorine atoms from three unique 2,4,6-trichlorobenzoic acid ligands on neighboring units (Cl1, Cl5, Cl9). Halogen–halogen interactions are known to preferentially adopt one of two arrangements that minimize overlap of regions of negative electrostatic potential,[6] and the interactions in **4** are both classified as Type I interactions based on criteria delineated by *Desiraju* et al.[7] The two Cl–Cl interactions that comprise the bifurcated linkage are the Cl1–Cl5 Type I interaction at a distance of 3.2282(3) Å (92.2 % sum of the van der Waals radii) with θ_1 (C15–Cl1–Cl5) and θ_2 (C24–Cl5–Cl1) values of 158.17(1)° and 148.56(1)°, respectively, as well as the Type I interaction between Cl5 and Cl9 at a distance of 3.4533(4) Å (98.7 % sum of the van der Waals radii) with θ_1 (C33–Cl5–Cl9) and θ_2 (C24–Cl5–Cl9) values of 125.20(1)° and 123.86(1)°.

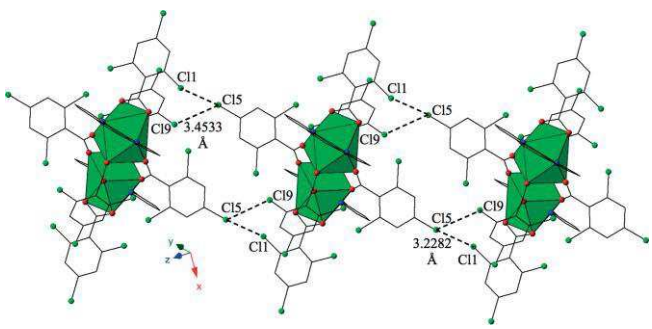

Figure 1. Complex **4** viewed as propagating along approximately the [1] direction. Bifurcated Type I Cl–Cl interactions that assemble dimers of **4** into 1D chain are displayed.

Further assembly of the dimers of **4** into a supramolecular 2D sheet in approximately the (100) plane is the result of three unique, localized Cl–π interactions.[8] Highlighted in Figure 2 is the "strongest" of the three interactions between the chlorine atom Cl2 and a carbon atom from the phen moiety (C12) on a neighboring chain. Halogen–π interaction strength criteria has been defined by *Reedijk* et al. and is determined via comparison to the corresponding sum of the van der Waals radii of the two interacting atoms (3.450 Å for chlorine and carbon).[9] The localized Cl2–C12 interaction is at a distance of 3.2956(4) Å, (95.5 % sum of the van der Waals radii), and supplementing the localized Cl2–C12 linkage are two additional "weaker" Cl–π interactions (Cl5–C18) and (Cl8–C4) (Table S4, Support-ing Information).

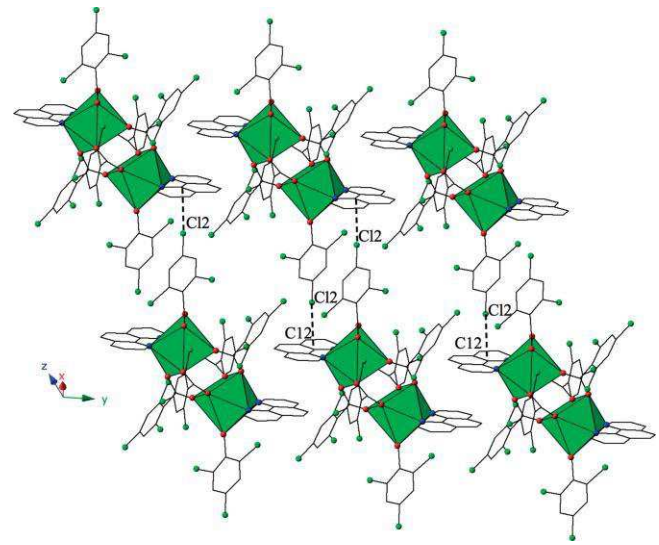

Figure 2. Complex **4** viewed in approximately the (100) plane highlighting one of three localized Cl–π interactions that further link dimers into supramolecular 2D sheet.

Structural Discussion

As complexes **1**–**10** were prepared using nearly identical reaction conditions to those used to produce the isostructural *Ln*-*p*-ClBA-phen complexes described previously,[5b] they provide an ideal platform to probe crystal engineering, specifically promoting synthons of choice, within lanthanide hybrid materials. In recent years our group has been interested in exercising some measure of control over non-covalent assembly in molecular lanthanide complexes. Initial efforts with *para*-functionalized halogen benzoic acid ligands and chelating N-donors (phen and 2,29:69,299-terpyridine) were promising,[1f,1g,5a,5b] yet assembly of the observed monomers and dimers proceeded via a wide array of supramolecular synthons (π–π, hydrogen bonding, *X*–π, *X*–*X*). More recently, we synthesized and characterized a series of rare-earth dimers and tetramers featuring 3,5-dichlorobenzoic acid and 2,29:69,299-terpyridine and for the first time noted a propensity for assembly to occur via halogen bonding interactions (specifically Cl–Cl or Cl–π) within rare-earth hybrid materials.[5d] In that

Table 1. Structural summary comparing *Ln*-*p*-ClBA-phen structure type III complexes[5b] with *Ln*-246triClBA-phen complexes (**1**–**10**).

	[*Ln*($C_{12}H_8N_2$)($C_7H_4ClO_2$)$_3H_2O$]$_2$ (Sm^{3+}-Lu^{3+}) [5b]	[*Ln*($C_{12}H_8N_2$)($C_7H_2Cl_3O_2$)$_3H_2O$]$_2$ (Sm^{3+}-Lu^{3+})
SBU	dimer	dimer
Ln CN(s)	8	8
Supramolecular interactions	Cl–π, π–π	Cl–Cl (32), Cl–π (33)
Dimensionality	2D	2D

study we speculated that increases in halogen bonding frequency were a result of an increased number of halogen atoms at the periphery of the tectons,[5d] and here we aimed to verify this hypothesis by producing a *Ln*-*p*-ClBA-phen structural analogue featuring 2,4,6-trichlorobenzoic acid (instead of *p*-ClBA) and directly comparing the supramolecular synthons each structure type utilizes for assembly.

In complexes **1**–**10**, each central Ln^{3+} metal atom (Ln^{3+} = Sm^{3+} – Lu^{3+}) is bound to a bidentate phen ligand, and then further coordinated to three crystallographically unique 2,4,6-trichlorobenzoic acid ligands that adopt either bidentate or bridging bidentate coordination modes. Lanthanide coordination numbers for **1**–**10** are eight and molecular arrangements about the central Ln^{3+} metal atom can be described as distorted square antiprismatic, as was observed in structure type III (Sm^{3+} – Lu^{3+}) *Ln*-*p*-ClBA-phen complexes described in our earlier study (Table 1).[5b] Whereas local coordination environments are unaffected by changes in the benzoic acid ligand, we note significant differences when comparing modes of assembly between *Ln*-*p*-ClBA-phen structure type III with *Ln*-246triClBA-phen structure type I (i.e. **1**–**10**). The *Ln*-*p*-ClBA-phen dimers described previously are linked via a single, unique localized Cl–π interaction and offset π–π inter-actions to form a supramolecular 2D sheet,[5b] whereas the *Ln*-246triClBA-phen dimers herein utilize bifurcated Type I Cl–Cl interactions along with three, unique localized Cl–π interactions to also form a supramolecular 2D sheet (Table 1, Figure S1, Supporting Information). This evolution in assembly from a single Cl–π interaction for the *Ln*-*p*-ClBA-phen dimers to a combination of five halogen bonding interactions (2 Cl–Cl, 3 Cl–π) for **1**–**10** suggests our hypothesis that an increased number of halogen atoms at the periphery of the tectons increases halogen bond frequency may be valid,[5d] yet in the absence of additional data points across other systems and rigorous theoretical treatment we hesitate to comment more definitively.

Luminescence

Solid-state photoluminescence spectra (room temperature) were collected for complexes **1** (Sm^{3+}), **2** (Eu^{3+}), **4** (Tb^{3+}), **5** (Dy^{3+}), **7** (Er^{3+}), and **9** (Yb^{3+}). The photoluminescence behavior of complexes **6** (Ho^{3+}) and **8** (Tm^{3+}) were also probed in the near-IR and visible regions, respectively, yet the characteristic peaks of these two lanthanide ions were not observed. All complexes were excited at wavelengths corresponding to the absorption maxima of the phen ligand, which functions as the sensitizing antenna for the Ln^{3+} complexes described herein.

For complex **1** (Sm^{3+}), the characteristic $^4G_{5/2}$ ^6H_J (J = 5/2 9/2) spectral bands were observed at approximately 562, 595, and 642 nm upon excitation at 356 nm along with some residual ligand fluorescence signal from the phen antenna, which also results in slight peak broadening of the characteristic Sm^{3+} transitions (Figure 3).

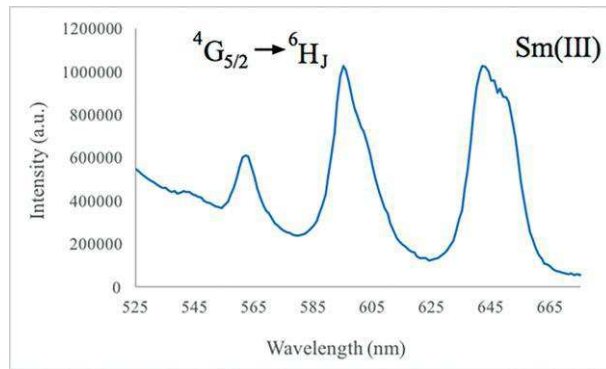

Figure 3. Solid-state emission spectrum for Sm^{3+} complex **1**.

The characteristic $^5D_0$ ^7F_J (J = 0 3) transitions of Eu^{3+} were observed for complex **2** upon excitation at 343 nm (Fig-ure 4). Dominating the spectrum of **2** is the hypersensitive $^5D_0$ $^7F_2$ transition, which is split into three peaks at ca. 611, 615, and 621 nm, and it is this spectral band that is responsible for the characteristic red luminescence of Eu^{3+} materials. Additionally, the $^5D_0$ $^7F_2$ transition is significantly more in-tense than the $^5D_0$ $^7F_1$ magnetic-dipole transition, which coupled with the splitting observed in both of these transitions and the stronger than usual $^5D_0$ $^7F_0$ signal, indicate that the central Eu^{3+} metal atom in **2** lies at a low-symmetry site that is not on an inversion center.[10]

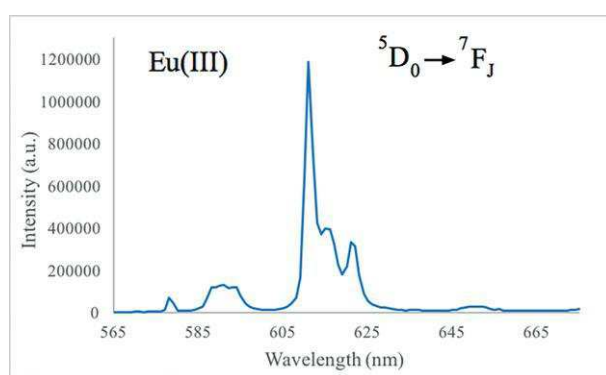

Figure 4. Solid-state emission spectrum for Eu^{3+} complex **2**.

The four spectral bands of the complex **4** (Tb^{3+}) at 487, 542, 583, and 619 nm correspond to the $^5D_4$ ^7F_J (J = 6 3) electronic transitions of the Tb^{3+} ion (Figure 5). The strongest observed transition was the $^5D_4$ $^7F_5$ band ca. 542 nm, which

is responsible for the characteristic green color of Tb^{3+} emission. Moreover, the emission spectrum for complex **5** (Dy^{3+}) reveals the expected Dy^{3+} centered peaks superimposed upon a residual fluorescence signal from the phen antenna (Fig-ure 5). The peaks at 478 and 573 nm can be assigned to the $^4F_{9/2}$ $^4H_{15/2}$ magnetic-dipole and $^4F_{9/2}$ $^4H_{13/2}$ electric-dipole transitions of Dy^{3+}, respectively.

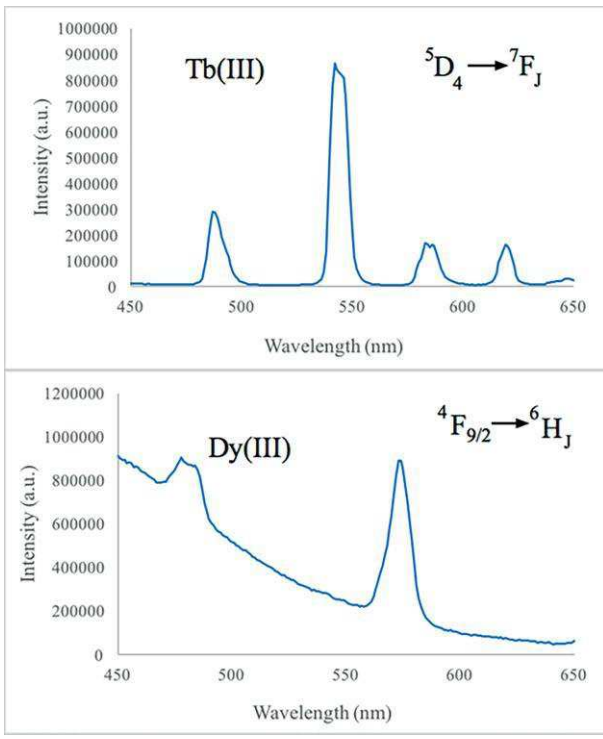

Figure 5. (Top) Solid-state emission spectrum for Tb^{3+} complex **4**. (Bottom) Solid-state emission spectrum for Dy^{3+} complex **5**.

The near-IR luminescence spectra of **7** (Er^{3+}) and **9** (Yb^{3+}) were collected after excitation at 355 nm via Nd:YAG pulsed laser, and feature bands at 1004 nm and 1535 nm correspond-ing to the characteristic $^2F_{5/2}$ $^2F_{7/2}$ and $^4I_{13/2}$ $^4I_{15/2}$ transi-tions of Yb^{3+} and Er^{3+}, respectively (Figure 6). For **9**, the structured peak ca. 980 nm is also assigned to the $^2F_{5/2}$ $^2F_{7/2}$ transition, and the peak splitting and variation in the intensities of the spectrum of **9** is likely the result of ligand-field M_J splitting of the $^2F_{7/2}$ state of Yb^{3+}.[11]

Time-resolved emission measurements were also obtained on solid samples of **1**, **2**, **4**, **5**, **6**, **7**, and **9** (Table 2). In most cases the decay profiles were best fitted to more than one exponential component, thus yielding more than one lifetime value. Such an observation is indicative of subtle variation in the Ln^{3+} coordination environment locale that is often inherent to solid-state samples. In fact, in the cases of **1** (Sm^{3+}) and **4** (Tb^{3+}), the lifetime data fitted best (as statistically judged by the residual errors) to a tri-exponential decay yielding three distinct lifetime values. Of the samples, the Eu^{3+}system (**2**) showed the longest lifetime in the millisecond domain, consistent with previous observations for emissive Eu^{3+} phosphors.[12] All other obtained lifetimes broadly fall into the expected ranges for each respective central Ln^{3+} atom, although

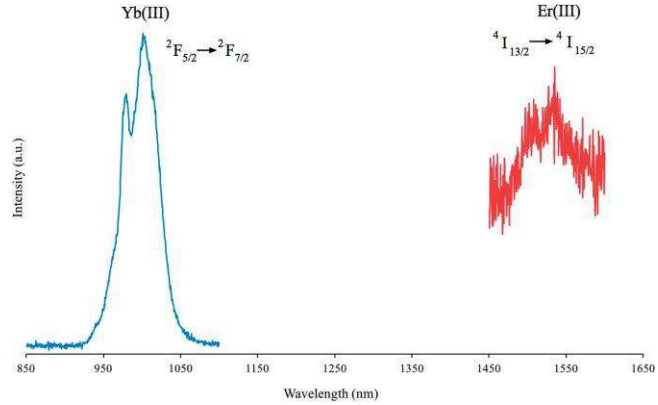

Figure 6. Near-IR solid-state emission spectra for Er^{3+} complex **7** and Yb^{3+} complex **9**.

it is notable that for the Tb^{3+} species (**4**), sub-millisecond values were obtained, suggestive of significant quenching of the emitting state [given that the energy level of the phen triplet excited state (ca. 21100 cm^{-1})[13] resides ,2000 cm^{-1} above the accepting $^5D_4$ state of Tb^{3+}, the possibility of back energy transfer should not be discounted].

Table 2. Visible and near-IR luminescent lifetimes of selected Ln-2,4,6-trichlorobenzoic acid-1,10-phenanthroline materials.

Complex	τ_{obs} (sec)
1 (Sm^{3+})	1.81E-6, 1.10E-5, 5.66E-5
2 (Eu^{3+})	4.48E-4, 1.15E-3
4 (Tb^{3+})	2.41E-5, 5.35E-5, 1.60E-4
5 (Dy^{3+})	1.53E-6, 1.18E-5
6 (Ho^{3+})	H 25E-9
7 (Er^{3+})	2.16E-6, 5.53E-6
9 (Yb^{3+})	1.61E-5

Magnetism

Direct current (dc) magnetic measurements were performed on complexes **5** and **7** between 1.8 and 300 K, with an applied dc field of 1000 Oe. The temperature dependence of the χT product for all samples can be observed in Figure 7. At room temperature, the observed χT values are as follows: 27.02 $cm^3 \cdot K \cdot mol^{-1}$ for **5** and 19.77 $cm^3 \cdot K \cdot mol^{-1}$ for **7**. The χT value for the **5** is slightly lower than the theoretical value of 28.34 $cm^3 \cdot K \cdot mol^{-1}$ for two non-interacting Dy^{3+} ions ($^6H_{15/2}$, $S = 5/2$, $L = 5$, $g = 4/3$, $\chi T = 14.17$ $cm^3 \cdot K \cdot mol^{-1}$) and similarly, the χT value for the **7** is also slightly lower than the theoretical

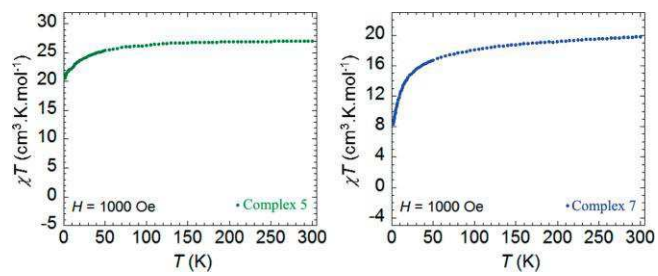

Figure 7. Temperature dependence of the χT product at 1000 Oe for complexes **5** (Dy^{3+}) and **7** (Er^{3+}).

value of 22.96 $cm^3 \cdot K \cdot mol^{-1}$ for two non-interacting Er^{3+} ions ($^4I_{15/2}$, $S = 3/2$, $L = 6$, $g = 6/5$, $\chi T = 11.48$ $cm^3 \cdot K \cdot mol^{-1}$). For **5** and **7** the χT product remains fairly stable upon a decrease in temperature until approximately 80 K, where a gradual decrease can be observed prior to a more dramatic drop to 20.59 $cm^3 \cdot K \cdot mol^{-1}$ for **5** and to 8.35 $cm^3 \cdot K \cdot mol^{-1}$ for **7** (at 1.8 K). The consistent negative deviation of the χT product is most likely attributed to a combination of possible factors, such as: inherent magnetic anisotropy present in Dy^{3+} and Er^{3+}, antiferromagnetic intramolecular interactions, and/or depopulation of the M_J states.

To verify the presence of magnetic anisotropy, isotherm magnetization data was collected between 1.8 and 7 K for each complex (Figure S2, Supporting Information). *M* vs. *H* data below 7 K demonstrates a rapid increase in the magnetization at low magnetic fields and a shoulder develops below 1 T, followed by a gradual increase of *M* at 1.8 K reaching 11.18 μ_B (**5**) and 9.57 μ_B (**7**) at 7 T without magnetic saturation. The *M* vs. *H*/*T* data also displays similar behavior for both complexes, where at high fields there is no saturation or overlay onto a single master curve, which is suggestive of the presence of non-negligible magnetic anisotropy and/or low-lying excited states. Despite *M* vs. *H*/*T* data indicating the possible presence of magnetic anisotropy, complex **5** was investigated in greater detail to probe any potential single molecule magnet (SMM) behavior, and thus out-of-phase (χ99) magnetic susceptibility was investigated. Under zero applied dc field there was no temperature dependent signal observed, however, under an ap-

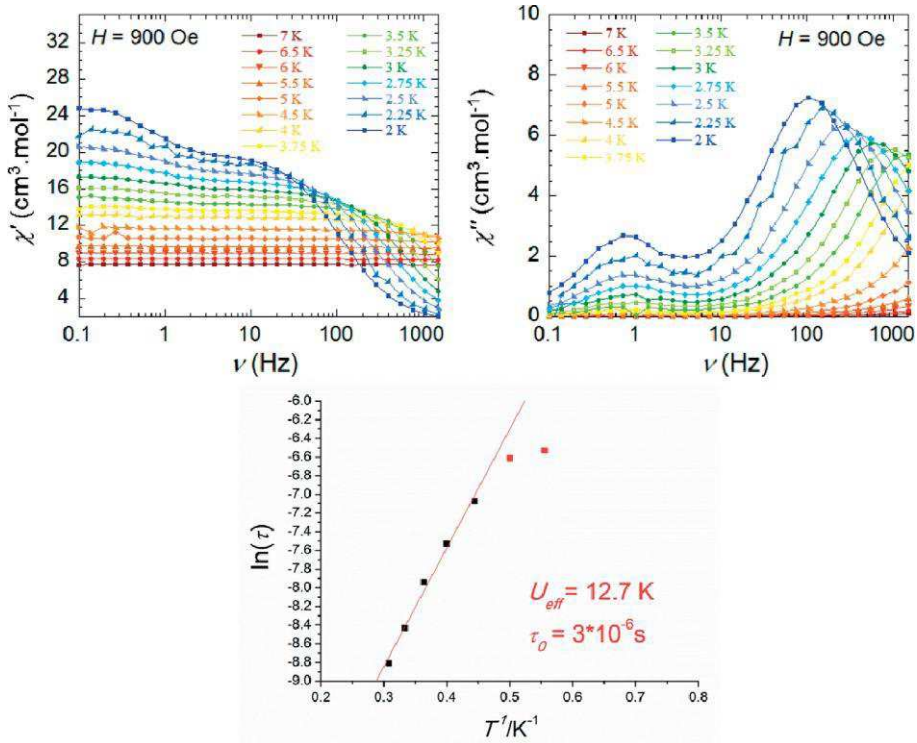

Figure 8. (Top) Frequency dependence of the in-phase (χ9) (left) and out-of-phase (χ99) (right) susceptibilities at 900 Oe for complex **5**. (Bottom) Relaxation time of the magnetization ln(τ) vs. T^{-1} for (Arrhenius plot using ac data) under 900 Oe applied field (fast relaxation process). The solid red line corresponds to the fit.

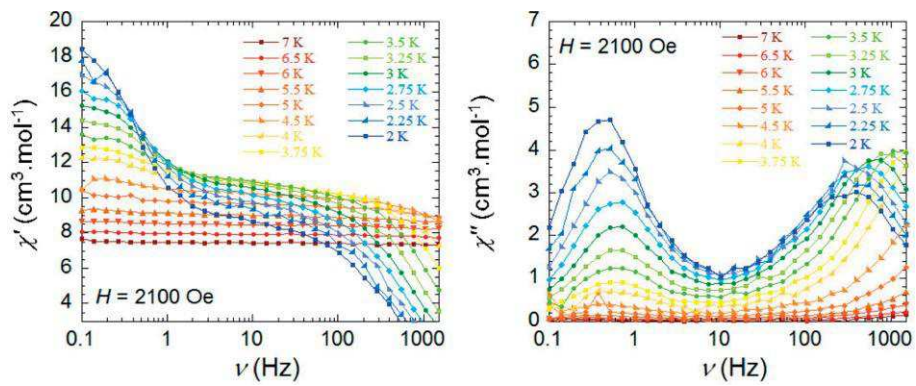

Figure 9. Frequency dependence of the in-phase (χ9) (left) and out-of-phase (χ99) (right) susceptibilities at 2100 Oe for complex **5**.

plied dc field of 1000 Oe a signal was observed for **5**. Such behavior is indicative of significant quantum tunneling of the magnetization (QTM) occurring in the absence of an applied magnetic field. The dynamic behavior of **5** was therefore investigated through ac susceptibility measurements at various frequencies (0.1–1500 Hz) between 7 and 1.9 K and under optimized applied dc fields of 900 Oe and 2100 Oe, respectively. Frequency dependent in-phase (χ9) and out-of-phase (χ99) mag-netic susceptibility plots for the fast relaxation process (opti-mal field: 900 Oe) can be observed in Figure 8.

The effective energy barrier and relaxation time for **5** were obtained through fitting the data using the Arrhenius equation [$\tau = \tau_0 \exp(U_{eff}/kT)$], which elicited a value of U_{eff} = 12.7 K (τ_0 = 3 310^{-6} s) (Figure 8). Frequency dependent in-phase (χ9) and out-of-phase (χ99) magnetic susceptibility plots for the slow relaxation process (optimal field: 2100 Oe) can be observed in Figure 9, yet it should be noted that minimal shift was observed in the peak maxima indicative of the presence of significant QTM, thus an energy barrier for this relaxation process could not be ascertained.

Conclusions

The syntheses and crystal structures of ten molecular lanthanide complexes featuring 2,4,6-trichlorobenzoic acid and 1,10-phenanthroline are reported, and their means of supramolecular assembly have been detailed and compared to isostructural *Ln-p*-chlorobenzoic acid-phen analogues. Visible and near-IR luminescence spectra and observed lifetimes (where possible) were detailed and the magnetic features of the Dy^{3+} (**5**) and Er^{3+} (**7**) dimers of the series were evaluated, where **5** was found to display slow relaxation of the magnetization under optimal applied dc fields. The primary aim of this study was to assess the hypothesis that promotion of halogen bonding interactions could be made possible by increasing halogen atoms at the periphery of tectons, and direct comparison of *Ln*-246triClBA-phen and *Ln-p*-ClBA-phen analogues verified this premise. Assembly of *Ln*-246triClBA-phen complexes into 2D networks was a result five halogen bonding interac-tion, whereas *Ln-p*-ClBA-phen complexes are known to only utilize one halogen bonding interaction for assembly.[5b] Fol-low up studies utilizing computational efforts to enhance understanding of non-covalent assembly in lanthanide hybrid materials are in development.

Experimental Section

Materials and Methods: $Sm(NO_3)_3{\cdot}6H_2O$ (Alfa Aesar, 99.9 %), $Ln(NO_3)_3{\cdot}xH_2O$ (where *Ln* = Eu^{3+}, Gd^{3+}, Tb^{3+}, Dy^{3+}, Ho^{3+}, Er^{3+}, and Yb^{3+}, *x* = 1,5 or 6, Strem Chemicals, 99.9 %), $Ln(NO_3)_3{\cdot}xH_2O$ (where *Ln* = Tm^{3+}, Lu^{3+}, *x* = 1 or 5, Sigma Aldrich, 99.9 %), 2,4,6-trichlorobenzoic acid (Alfa Aesar, 94 %), and 1,10-phenanthroline (Alfa Aesar, Fischer, 98 %) were used for syntheses as received.

Synthesis: Complexes **1**–**10** were all synthesized via hydrothermal methods in a 23 mL Teflon-lined autoclave at an oven temperature of 150 °C. A mixture of Ln^{3+} nitrate hydrate [$Ln(NO_3)_3{\cdot}xH_2O$, *Ln* = Sm^{3+} – Lu^{3+}, *x* = 1, 5 or 6] (**1**–**10**), 2,4,6-trichlorobenzoic acid ($C_7H_2Cl_3O_2$), 1,10-phenanthroline ($C_{12}H_8N_2$), and distilled water (mo-lar ratio 1:2:2:826) was heated for 48 h under autogenous pressure. Upon removal from the oven, the samples were allowed to cool to ambient temperature over 4 h and opened after approximately 12 h. Colorless small, block crystals were obtained from the bulk product after decanting the supernatant liquor, washing three times with dis-tilled water and ethanol, and air-drying at room temperature overnight.

X-ray Structure Determination: Single crystals from each bulk sam-ple were isolated and mounted on MiTeGen micromounts. Structure determination for each of the single crystals was achieved by collecting reflections using 0.5° ω scans with a Bruker SMART diffractometer furnished with an APEX II CCD detector using Mo-K_α (λ = 0.71073 Å) radiation at low temperature [100(2) K]. Integration was done using the SAINT software package[14] that is a part of the APEX II software suite[15] and absorption corrections were applied using SADABS.[16] Complexes **1**–**10** were solved via direct methods using SIR 92.[17] All ten complexes were refined using SHELXL-2014[18] in the WinGX[19] software suite. In each structure, all non-hydrogen

Table 3. Crystallographic data for complexes **1**–**5**.

	1	**2**	**3**	**4**	**5**
Chem. formula	$C_{66}H_{28}Cl_{18}N_4O_{12}Sm_2$	$C_{66}H_{28}Cl_{18}N_4O_{12}Eu_2$	$C_{66}H_{28}Cl_{18}N_4O_{12}Gd_2$	$C_{66}H_{28}Cl_{18}N_4O_{12}Tb_2$	$C_{66}H_{28}Cl_{18}N_4O_{12}Dy_2$
Formula weight	2007.72	2010.94	2021.52	2024.86	2032.02
Crystal system	triclinic	triclinic	triclinic	triclinic	triclinic
Space group	*P*1	*P*1	*P*1	*P*1	*P*1
a /Å	12.1756(5)	12.1482(12)	12.1293(11)	12.1167(12)	12.0799(11)
b /Å	12.2082(5)	12.1863(12)	12.1664(11)	12.1389(13)	12.1173(11)
c /Å	13.3569(6)	13.3646(13)	13.3757(12)	13.3851(14)	13.3690(12)
α /°	111.798(11)	111.760(1)	111.683(10)	111.680(4)	111.686(8)
β /°	97.556(9)	97.749(2)	97.870(11)	98.049(3)	98.061(7)
γ /°	102.236(10)	102.065(2)	101.984(11)	101.857(4)	101.599(8)
V /Å^3	1752.56(19)	1747.2(3)	1743.9(3)	1739.2(3)	1731.1(3)
Z	1	1	1	1	1
T /K	100(2)	100(2)	100(2)	100(2)	100(2)
λ (Mo-K_α)	0.71073	0.71073	0.71073	0.71073	0.71073
D_{calc} /g·cm^{-3}	1.902	1.911	1.925	1.933	1.949
μ /mm^{-1}	2.411	2.533	2.640	2.774	2.903
R_{int}	0.0218	0.0475	0.0342	0.0669	0.0320
R_1 [I . 2σ(I)]	0.0189	0.0322	0.0232	0.0407	0.0273
wR_2 [I . 2σ(I)]	0.0472	0.0648	0.0522	0.0745	0.0665

Table 4. Crystallographic data for complexes **6**–**10**.

	6	**7**	**8**	**9**	**10**
Chem. formula	$C_{66}H_{28}Cl_{18}N_4O_{12}Ho_2$	$C_{66}H_{28}Cl_{18}N_4O_{12}Er_2$	$C_{66}H_{28}Cl_{18}N_4O_{12}Tm_2$	$C_{66}H_{28}Cl_{18}N_4O_{12}Yb_2$	$C_{66}H_{28}Cl_{18}N_4O_{12}Lu_2$
Formula weight	2036.88	2041.54	2044.88	2053.10	2056.96
Crystal system	triclinic	triclinic	triclinic	triclinic	triclinic
Space group	*P*1	*P*1	*P*1	*P*1	*P*1
a /Å	12.0965(15)	12.0743(10)	12.0605(6)	12.0459(13)	12.0278(8)
b /Å	12.0974(15)	12.0790(11)	12.0645(6)	12.0538(13)	12.0456(8)
c /Å	13.4071(17)	13.4133(11)	13.4156(7)	13.4306(14)	13.4320(9)
α /°	111.562(12)	98.507(6)	98.655(7)	98.796(10)	98.857(4)
β /°	98.376(11)	111.550(6)	111.502(8)	111.515(11)	111.466(5)
γ /°	101.696(12)	101.596(7)	101.484(7)	101.379(11)	101.346(5)
V /Å^3	1733.8(4)	1728.8(3)	1725.53(18)	1723.5(4)	1720.4(2)
Z	1	1	1	1	1
T /K	100(2)	100(2)	100(2)	100(2)	100(2)
λ (Mo-K_α)	0.71073	0.71073	0.71073	0.71073	0.71073
D_{calc} /g·cm^{-3}	1.951	1.961	1.968	1.978	1.985
μ /mm^{-1}	3.025	3.173	3.318	3.461	3.618
R_{int}	0.0551	0.0617	0.0347	0.0403	0.0338
R_1 [I . 2σ(I)]	0.0328	0.0382	0.0245	0.0248	0.0261
wR_2 [I . 2σ(I)]	0.0696	0.0715	0.0550	0.0598	0.0542

atoms were located via difference Fourier maps and refined anisotropically. Aromatic hydrogen atoms were placed at their idealized positions by employing the HFIX43 instruction in SHELXL-2014 and allowed to ride on the coordinates of their parent carbon atom [(U_{iso}) fixed at 1.2U_{eq}]. All figures were prepared with CrystalMaker.[20] Data collection and refinement details are included in Table 3 for complexes **1**–**5** and Table 4 for complexes **6**–**10**.

Powder X-ray Diffraction: Powder X-ray diffraction (PXRD) data on the bulk reaction product of complexes **1**–**10** (Figures S3–S12, Supporting Information) were used to examine the bulk purity of each sample. All data were collected with a Rigaku Miniflex (Cu-K_α, 2θ = 3–60°) and were analyzed using the JADE software program.[21]

Luminescence Measurements: Room temperature solid-state visible luminescence measurements were obtained for complexes **1**, **2**, **4**, and **5** with a Horiba JobinYvon Fluorlog-3 spectrophotometer. Near-IR photophysical data for **7** and **9** were obtained with a Horiba JobinYvon Fluorolog-3 spectrometer fitted with a Hamamatsu R5509-73 detector (cooled to –77 °C using C9940 housing). All data were manipulated using the FluoroEssence software package and final plots of the solid-state spectra were made in Microsoft Excel. Lifetime data were collected for **2**, **6**, **7**, and **9** with a Horiba JobinYvon Fluorolog-3 spectrometer fitted with a JY TBX picoseconds photodetection module and a Continuum Minilite Nd:YAG pulsed laser configured for 355 nm output, whereas data for **1**, **4**, and **5** were collected with a Horiba JobinYvon Fluorolog-3 spectrometer adapted for time-correlated single photon counting (TCSPC) and multichannel scaling (MCS) measure-ments using a Xenon flash lamp as the light source. Lifetime profiles for all seven complexes were obtained using the JobinYvon FluoroHub single photon counting module and the data were fit using DAS6 soft-ware.

Magnetic Measurements: Magnetic measurements were performed with a Quantum Design SQUID magnetometer MPMS-XL7, operating between 1.8 and 300 K for dc-applied fields ranging from –7 to 7 T. Susceptibility measurements were performed on powder samples of 27.9 mg of complex **5** (Dy^{3+}) and 14.7 mg of complex **7** (Er^{3+}), each wrapped within a polyethylene membrane. Direct current (dc) susceptibility measurements were performed at 1000 Oe. The magnetization data was initially collected at 100 K to check for ferromagnetic impurities, found to be absent in all samples.

Crystallographic data (excluding structure factors) for the structures in this paper have been deposited with the Cambridge Crystallographic Data Centre, CCDC, 12 Union Road, Cambridge CB21EZ, UK. Copies of the data can be obtained free of charge on quoting the depository numbers CCDC-1571878, CCDC-1571879, CCDC-1571880, CCDC-1571881, CCDC-1571882, CCDC-1571883, CCDC-1571884, CCDC-1571885, CCDC-1571886, and CCDC-1571887 for complexes **1**–**10**, respectively (Fax: +44-1223-336-033; E-Mail: deposit@ccdc.cam.ac.uk, http://www.ccdc.cam.ac.uk).

Supporting Information (see footnote on the first page of this article): X-ray crystallographic files in CIF format, ORTEP figures of all com-plexes, PXRD spectra of all complexes, additional magnetism data for complexes **5** and **7**, additional comparisons of halogen bonding in *Ln*-*p*-ClBA-Phen and *Ln*-2,4,6-triClBA-Phen complexes, and tables of selected supramolecular interaction distances and bond lengths.

Acknowledgements

This material is based upon work supported as part of the Materials Science of Actinides, an Energy Frontier Research Center funded by the U.S. Department of Energy, Office of Science, Office of Basic Energy Sciences, under Award Number DE-SC0001089. K. P. C. would also like to acknowledge George Washington University for a Presidential Merit Fellowship award. Additionally, the authors are grateful to *J. August Ridenour* for assistance with luminescence lifetime measurements.

Keywords: Molecular lanthanide complexes; Lanthanide tectons; Lanthanides

References

[1] a) J.-C. G. Bünzli, C. Piguet, *Chem. Rev.* **2002**, *102*, 1897–1928; b) S. J. Bradberry, A. J. Savyasachi, M. Martinez-Calvo, T. Gunnlaugsson, *Coord. Chem. Rev.* **2014**, *273–274*, 226–241; c) A. de Bettencourt-Dias, P. S. Barber, S. Viswanathan, *Coord. Chem. Rev.* **2014**, *273–274*, 165–200; d) K. P. Carter, C. L. Cahill, in *Handbook on the Physics and Chemistry of Rare Earths*, vol.

47 (Eds.: J.-C. G. Bünzli, V. K. Pecharsky), Elsevier, Amsterdam, **2015**, pp. 147–208; e) D. E. Barry, D. F. Caffrey, T. Gunnlaugsson, *Chem. Soc. Rev.* **2016**, *45*, 3244–3274; f) J. A. Ridenour, K. P. Carter, R. J. Butcher, C. L. Cahill, *CrystEngComm* **2017**, *19*, 1172–1189; g) J. A. Ridenour, K. P. Carter, C. L. Cahill, *CrystEngComm* **2017**, *19*, 1190–1203.

[2] a) J.-C. G. Bünzli, *Chem. Lett.* **2009**, *38*, 104–109; b) J.-C. G. Bünzli, *J. Luminesc.* **2016**, *170*, 866–878; c) A. J. Amoroso, I. A. Fallis, S. J. A. Pope, *Coord. Chem. Rev.* **2017**, *340*, 198–219.

[3] a) C. Andraud, O. Maury, *Eur. J. Inorg. Chem.* **2009**, *2009*, 4357–4371; b) G.-L. Law, K.-L. Wong, K.-K. Lau, S.-T. Lap, P. A. Tanner, F. Kuo, W.-T. Wong, *J. Mater. Chem.* **2010**, *20*, 4074–4079; c) R. Medishetty, J. K. Zareba, D. Mayer, M. Samoc, R. A. Fischer, *Chem. Soc. Rev.* **2017**, *46*, 4976–5004.

[4] a) J. Luzon, R. Sessoli, *Dalton Trans.* **2012**, *41*, 13556–13567; b) D. N. Woodruff, R. E. P. Winpenny, R. A. Layfield, *Chem. Rev.* **2013**, *113*, 5110–5148; c) A.-J. Hutchings, F. Habib, R. J. Holmberg, I. Korobkov, M. Murugesu, *Inorg. Chem.* **2014**, *53*, 2102–2112; d) K. L. M. Harriman, M. Murugesu, *Acc. Chem. Res.* **2016**, *49*, 1158–1167.

[5] a) K. P. Carter, S. J. A. Pope, C. L. Cahill, *CrystEngComm* **2014**, *16*, 1873–1884; b) K. P. Carter, C. H. F. Zulato, C. L. Cahill, *CrystEngComm* **2014**, *16*, 10189–10202; c) K. P. Carter, C. H. F. Zulato, E. M. Rodrigues, S. J. A. Pope, F. A. Sigoli, C. L. Cahill, *Dalton Trans.* **2015**, *44*, 15843–15854; d) K. P. Carter, K. E. Thomas, S. J. A. Pope, R. J. Holmberg, R. J. Butcher, M. Murugesu, C. L. Cahill, *Inorg. Chem.* **2016**, *55*, 6902–6915.

[6] a) L. C. Gilday, S. W. Robinson, T. A. Barendt, M. J. Langton, B. R. Mullaney, P. D. Beer, *Chem. Rev.* **2015**, *115*, 7118–7195; b) G. Cavallo, P. Metrangolo, R. Milani, T. Pilati, A. Priimagi, G. Resnati, G. Terraneo, *Chem. Rev.* **2016**, *116*, 2478–2601.

[7] a) G. R. Desiraju, R. Parthasarathy, *J. Am. Chem. Soc.* **1989**, *111*, 8725–8726; b) A. Mukherjee, S. Tothadi, G. R. Desiraju, *Acc. Chem. Res.* **2014**, *47*, 2514–2524.

[8] D. Schollmeyer, O. V. Shishkin, T. Ruhl, M. O. Vysotsky, *CrystEngComm* **2008**, *10*, 715–723.

[9] T. J. Mooibroek, P. Gamez, J. Reedijk, *CrystEngComm* **2008**, *10*, 1501–1515.

[10] a) M. O. Rodrigues, N. B. da Costa Junior, C. A. de Simone, A. A. S. Araujo, A. M. Brito-Silva, F. A. A. Paz, M. E. de Mesquita, S. A. Junior, R. O. Freire, *J. Phys. Chem. B* **2008**, *112*, 4204–4212; b) N. M. Shavaleev, R. Scopelliti, F. Gumy, J.-C. G. Bünzli, *Inorg. Chem.* **2009**, *48*, 6178–6191; c) J. A. Smith, M. A. Singh-Wilmot, K. P. Carter, C. L. Cahill, A. J. Lough, C. S. Knee, *New J. Chem.* **2016**, *40*, 7338–7349.

[11] a) R. F. Ziessel, G. Ulrich, L. Charbonnière, D. Imbert, R. Scopel-liti, J.-C. G. Bünzli, *Chem. Eur. J.* **2006**, *12*, 5060–5067; b) N. M. Shavaleev, R. Scopelliti, F. Gumy, J.-C. G. Bünzli, *Inorg. Chem.* **2009**, *48*, 7937–7946.

[12] a) J.-C. G. Bünzli, A.-S. Chauvin, H. K. Kim, E. Deiters, S. V. Eliseeva, *Coord. Chem. Rev.* **2010**, *254*, 2623–2633; b) M. Andrews, B. M. Kariuki, S. J. A. Pope, *Polyhedron* **2011**, *30*, 2055–2061.

[13] V. I. Tsaryuk, K. P. Zhuravlev, A. V. Vologzhanina, V. A. Kudrya-shova, V. F. Zolin, *J. Photochem. Photobiol. A: Chem.Chem.* **2010**, *211*, 7–19.

[14] *SAINT*, Bruker AXS Inc., Madison, WI, USA, **2007**.

[15] *APEXII*, 2.3 ed., Bruker AXS Inc., Madison, WI, USA, **2008**.

[16] L. Krause, R. Herbst-Irmer, G. M. Sheldrick, D. Stalke, *J. Appl. Crystallogr.* **2015**, *48*, 3–10.

[17] A. Altomare, G. Cascarano, C. Giacovazzo, A. Guagliardi, M. C. Burla, G. Polidori, M. Camalli, *J. Appl. Crystallogr.* **1994**, *27*, 435–435.

[18] G. Sheldrick, *Acta Crystallogr., Sect. C* **2015**, *71*, 3–8.

[19] L. Farrugia, *J. Appl. Crystallogr.* **2012**, *45*, 849–854.

[20] *CrystalMaker*, 8.2.2 ed., Crystal Maker Software Limited, Bicester, England, **2009**.

[21] *JADE*, 6.1 ed., Materials Data Inc., Livermore, CA, USA, **2003**.